Drastic effect of the peptide sequence on the copper-binding properties of tripeptides and the electrochemical behaviour of their copper(II) complexes

Silvia Mena, Andrea Mirats, Ana B. Caballero,[b] [a] Gonzalo Guirado,*[a] Leoní A. Barrios,[b] Simon J. Teat,[c] Luis Rodriguez-Santiago,[a] Mariona Sodupe,*[a] and Patrick Gamez*[b,d,e]

[a] Departament de Química, Universitat Autònoma de Barcelona, 08193 Bellaterra, Barcelona, Spain

[b] Departament de Química Inorgànica i Orgànica, Universitat de Barcelona, Martí i Franquès 1-11, 08028 Barcelona, Spain

[c] Advanced Light Source, Lawrence Berkeley National Lab, 1 Cyclotron Road, Berkeley, California 94720, United States

[d] Catalan Institution for Research and Advanced Studies, Passeig Lluís Companys 23, 08010 Barcelona, Spain

[e] Institute of Nanoscience and Nanotechnology (IN2UB), Universitat de Barcelona

Abstract

The binding and electrochemical properties of the complexes **Cu^{II}–HAH**, **Cu^{II}–HWH**, **Cu^{II}–Ac-HWH**, **Cu^{II}–HHW** and **Cu^{II}-WHH** have been studied by using NMR and UV-VIS spectroscopies, cyclic voltammetry (CV) and density functional calculations. The results obtained highlight the importance of the peptidic sequence on the coordination properties and, consequently, on the redox properties of their Cu(II) complexes. For **Cu^{II}–HAH** and **Cu^{II}–HWH**, no cathodic processes are observed up to –1.2 V; i.e., the complexes exhibit very high stability towards copper reduction. This behaviour is associated with the formation of a very stable square-planar (5,5,6)-membered chelate rings (ATCUN motif), which encloses two deprotonated amides. In contrast, for non-ATCUN **Cu^{II}–Ac-HWH**, **Cu^{II}–HHW** complexes, simulations seem to indicate that only one deprotonated amide is enclosed in the coordination sphere. In these cases, the main electrochemical feature is a reductive irreversible one electron-transfer process from Cu(II) to Cu(I), accompanied with structural changes of the metal coordination sphere and reprotonation of the amide. Finally, for **Cu^{II}–WHH,** two major species have been detected: one at low pH (< 5), with no deprotonated amides, and another one at high pH (> 10) with an ATCUN motif, both species coexisting at intermediate pH. The present study shows that the use of CV, using glassy carbon as a working electrode, is an ideal and rapid tool for the determination of the redox properties of Cu(II) metallopeptides.

INTRODUCTION

The amino terminal copper(II)- and nickel(II)-binding (ATCUN) motif is a peptidic sequence of type Xaa–Xaa–His (Xaa = any amino acid), which was first identified in metal-transport albumins,[1] including human serum albumin (HSA).[2] It was subsequently found in other natural proteins,[2-3] such as neuromedins C and K,[4] histatins[5] and human sperm protamine P2a.[6] The ATCUN metal-binding site, which is known for more than 55 years,[7] is characterized by a coordination donor-set composed of a free NH_2 terminus, two deprotonated amide nitrogen atoms from two amino acids at positions 1 and 2, and an imidazole from a histidine residue at the third position (Scheme 1).[8-9] These four N-atoms can specifically and strongly interact with copper(II) and nickel(II) ions, generating stable square-planar complexes (Scheme 1).[10] Nevertheless, the metal ions can be released in the presence of appropriate ligands;[11] therefore, this binding site is found in some metal transporters.[12]

Various other properties of copper(II)- and nickel(II)-bound ATCUN motifs have been reported (apart from metal transport), illustrating their great biological significance.[2] For instance, it has been shown that copper-ATCUN species are capable of cleaving DNA oxidatively in the presence of ascorbate,[13-14] most likely through a Fenton-like mechanism.[15-16] Nickel-ATCUN complexes can cleave DNA as well (even with sequence specificity),[17] but the process requires H_2O_2 instead of ascorbate (the nickel system being inactive with ascorbate).[18] Proteins can also be cleaved[19] and enzymes inactived[20] by metal-ATCUN compounds.

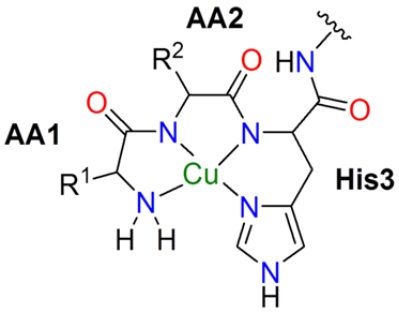

Scheme 1. Schematic representation of the ATCUN binding site.

Metal-ATCUN motifs have been involved in protein cross-linking;[21] for example, a Gly-Gly-His nickel(II)-ATCUN complex has been used to cross-link two proteins oxidatively, *via* the generation of highly active tyrosyl radicals mediated by a

nickel(III) oxo intermediate.[21-22] Such method has been applied for stitching viral capsids together.[23]

As a result of their attractive (biological) properties, ATCUN-based compounds have been developed as potential metallodrugs.[24-25] For example, a Gly-Gly-His copper(II)-ATCUN unit has been conjugated to a RNA-binding peptidic sequence, *i.e.* the YrFK-amide (Tyr–D-Arg–Phe–Lys-NH_2), to generate an active antiviral molecule (against hepatitis C virus).[26-27] However, it should also be mentioned here that metal-ATCUN-like motifs appear to be involved in severe diseases such as Alzheimer's disease,[28] where they may be implicated in the aggregation of pathogenic amyloid proteins.[29]

As exemplified above, the ATCUN ligand is of biological importance; therefore, one may wonder how frequently it is found in proteins. Actually, a simple search of the Protein Data Bank (PDB; accessed June 2017) for the sequence returns more than 12,500 entries. Hence, we wanted to investigate why Nature has chosen the sequence –H_2N–AA1–AA2–His3–, where AA1 and AA2 are not a histidine residue (*i.e.* ATCUN motif, see Scheme 1), to generate metal-binding proteins (*e.g.* metal transporters). Has the inclusion of a second histidine in the peptidic triad an important effect on the binding and physical properties (such as the redox properties) of the histidine-rich "ATCUN motif"? For this purpose, in the present study, tripeptides including two histidines (**H**) and one tryptophan (**W**) or alanine (**A**) have been selected to investigate the influence of an additional imidazole-containing residue on the copper-binding and redox properties of the well-known peptidic triad. Tryptophan (λ_{exc} = 280 nm; λ_{em} = 350 nm) has been chosen as a potential fluorescent reporter to allow metal-binding studies by fluorescence spectroscopy. Hence, the behaviour of five different (bi-histidine) tripeptides (Scheme 2), namely **HAH**, **HWH**, **Ac-HWH**, **HHW**, and **WHH** interacting with copper has been examined in great detail, both experimentally by means of cyclic voltammetry (CV) measurements and theoretically with DFT calculations. The tripeptide **HHW** has been selected to confirm the importance of the histidine residue at position 3 of the well-known ATCUN arrangement (Scheme 1). Similarly, the N-acetylated **Ac-HWH** peptide has been chosen to show the crucial role played by the N-terminal amino group for copper (or nickel) binding.

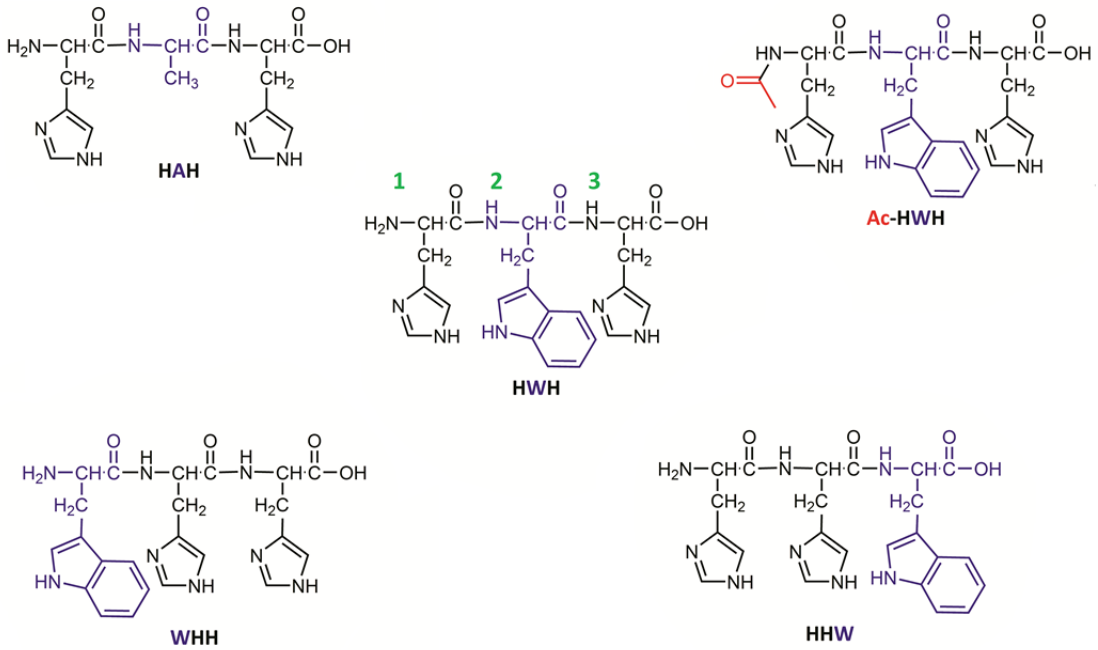

Scheme 2. Tripeptides used in the present study, namely L-histidyl-L-alanyl-L-histidine (**HAH**), L-histidyl-L-tryptophyl-L-histidine (**HWH**), N-acetyl-L-histidyl-L-tryptophyl-L-histidine (**Ac-HWH**), L-tryptophyl-L-histidyl-L-histidine (**WHH**) and L-histidyl-L-histidyl-L-tryptophane (**HHW**).

The thorough computational and experimental study reported herein clearly reveals that the simple addition of a histidine residue within the ATCUN motif considerably alters its metal-binding properties and the redox behaviour of the resulting copper complexes. Moreover, the position of this additional histidine residue within the sequence (namely at position 1 or 2) also has a profound effect on these properties.

MATERIALS AND METHODS

Chemicals. All solutions were prepared with Milli-Q (18 MΩ) water. Tripeptides **HWH**, **Ac-HWH**, **HAH**, **GWH**, **HHW** and **WHH** were customised by GeneCust (Luxembourg), and were received as hydrochloride salts with a purity ≥ 95 %. These peptides were used without further purification. Solutions and measurements were performed in 0.05 M TRIS + 0.1 M NaClO4, pH 7.4 buffer solution. Stock solutions of peptides (1 mM) were prepared by dissolving the peptides in the buffer solution. The concentrations of the prepared stock solutions were spectrophotometrically determined using the corresponding molar absorptivity coefficient of tryptophan (ε_{280} = 5690 M^{-1} cm^{-1}). $CuCl_2 \cdot 2H_2O$ was used as source of copper(II) ions in all the studies. In a typical

experiment, the Cu^{II}-peptide solution was obtained by adding the tripeptide to a buffer solution that contains a known concentration of Cu^{II} ions in a 1.1:1 ratio.

NMR studies. 1D and 2D NMR spectra of the Ac-His-Trp-His-OH (**Ac-HWH**) peptide were performed on a Bruker Avance III 400 MHz spectrometer, equipped with a 5 mm cryoprobe (Prodigy) broadband (CPPBBO BB-1 F/D) with gradients in Z, at the Centres Científics i Tecnológics of the Universitat de Barcelona (CCiTUB). Solvent suppression for the 1D experiments was achieved using a PRESAT pulse sequence. The NMR data were analyzed using MestReNova 9.1.0. Solutions of 10 mM peptide in D_2O were adjusted to pH 7.4, and measured with an insert containing a 5 mg mL^{-1} solution of [d_4] -3-(trimethylsilyl)propanoic acid (TSP) as an internal reference. The ^{1}H and ^{13}C signals of the peptide were assigned on the basis of ^{1}H-^{1}H COSY, ^{1}H-^{13}C HSQC, and ^{1}H-^{13}C HMBC experiments. In the presence of 0.01 equiv of $CuCl_2$, the intensity of the peptide NMR signals decreased by about 60%.

UV/Vis absorption spectroscopy. UV/Vis absorption spectra were recorded on Varian Cary 100 Scan spectrophotometer and on Hamamatsu L10290 spectrosphotometer with Bio-kine 32 V4.46 software, at room temperature, employing a 1cm pathlength cuvette.

Cyclic voltammetry (CV). Slow scan rates measurements (from 0.10 to 1.0 $V \bullet s^{-1}$) were recorded using a CHI660E Electrochemical Workstation CHInstruments using the Electrochemical Workstation software. CV at moderate scan rates (from 1.0 $V \bullet s^{-1}$ to 1000 $V \bullet s^{-1}$) were performed using a homemade solid-state ampifier potentiostat with positive feedback iR drop compensation connected to a TACUSSEL GSTP4 generator, a TECKTRONIX 2212 oscilloscope and to a plotter. The working electrode was glassy carbon disk (1 mm of diameter) and a Pt disk was used as counter electrode (< 1 mm of diameter). The reference electrode was an SCE electrode (0.24 V *vs* NHE) isolated in a ceramic bridge. Before any measurement of each voltammogram, the working electrode was carefully polished with DP-Nap-T polish disk (Struers), and washed carefully with ethanol. The electrochemical cell medium used was Milli-Q water with 0.05 M TRIS + 0.1 M $NaClO_4$ (pH 7.4) added as supporting electrolyte. All the electrochemical measurements were performed under nitrogen atmosphere.

Computational Calculations

Electronic structure calculations. All calculations were performed using the B3LYP-D3 method, that is, the B3LYP functional[30-32] plus the Grimme's correction (D3) for dispersion forces.[33] This method appropriately describes the coordination properties at

the metal site and the non-covalent interactions of the peptide. Moreover, the comparison between the results obtained with different functionals and electrochemical data nicely demonstrate that the method also provides balanced results for the calculation of the redox potentials of the Cu^{I}/Cu^{II} and Cu^{II}/Cu^{III} pairs. Main group elements were represented with the 6-311++G(d,p) basis set and Cu was represented with LANL2DZ effective core potential[34] and the associated LANL2TZ basis set,[35] supplemented with an *f* function.[36] Thermal corrections were evaluated at 298.15 K and 1 atm assuming unscaled harmonic vibrational frequencies and the rigid rotor approximation by standard statistical methods. Solvent effects were taken into account by using the SMD[37] implicit solvation model. Open-shell calculations were based on an unrestricted formalism. All calculations were done with the *Gaussian09* program.[38]

Standard potential calculations. The obtained Cu^{II}-L complexes were reduced and reoptimized to obtain the corresponding Cu^{I}-L ones. Thus, the SRP versus the SHE values were estimated considering the following semi-reactions:

$Cu^{II}\text{-}L_{(aq)} + 1e^{-} \rightarrow Cu^{I}\text{-}L_{(aq)}$ ΔG^{o}_{Cu}

and

$H^{+}_{(aq)} + 1e^{-} \rightarrow \frac{1}{2}\, H_{2(g)}$ ΔG^{o}_{SHE}

where ΔG^{o}_{Cu} and ΔG^{o}_{SHE} are the free energy changes for the semi-reactions, ignoring the electron. Thus, the SRP values are computed using the following equation:

$$E^{0}(Cu^{2+/+} - L) = -\left(\frac{\Delta G^{0}_{Cu} - \Delta G^{0}_{SHE}}{F}\right)$$

where *F* is the Faraday constant (23.061 kcal·V^{-1}·mol^{-1}). For the reduction of the proton in aqueous solution, the experimental value, ΔG^{SHE} = –99.9 kcal·mol^{-1}, was used.[39] Since the experimental potentials are estimated versus the *Saturated Calomelan Electrode* (SCE), while the theoretical potentials are calculated versus *Standard Hydrogen Electrode* (SHE), a correction of –0.24 V has been added to the theoretical potentials to compare with the experimental ones.

X-ray structure determination. Single crystals of **Cu^{II}–HHW** were obtained from a mixture of an equimolar amount of tripeptide and $CuCl_2$ in 100 mM HEPES pH 7.4. The resulting solution was filtered (a violet precipitate was separated) and a few drops of acetone were added in the filtrate. The solution was tightly closed; after a few days standing at room temperature, small prismatic violet crystals were isolated that were

suitable for X-ray diffraction studies. Data for complex **Cu^{II}–HHW** were collected on a Bruker PHOTON100 CMOS diffractometer at beamline 11.3.1 of the Advanced Light Source (synchrotron radiation, λ = 0.7749 Å) on a purple block at 100 K. Data reduction was done with SAINT.[40] The structures were solved by intrinsic phasing using SHELXT, and refined by full-matrix least squares on F^2 with SHELXL-2014.[41] Crystallographic and refinement parameters are summarized in Table S1, and selected bond distances and angles are listed in Table S2 (see SI). All details can be found in CCDC **1575952** that contain the supplementary crystallographic data for this paper. These data can be obtained free of charge from the Cambridge Crystallographic Data Center via https://summary.ccdc.cam.ac.uk/structure-summary-form.

RESULTS AND DISCUSSION

Electrochemical properties of peptides

Before starting the electrochemical studies of the considered peptides, we first analysed the electrochemical properties of tryptophan and histidine, since they enclose potentially active redox groups. That is; different solutions of tryptophan and histidine, 10 mM in 50 mM Tris/HCl pH 7 containing 0.1 M $NaClO_4$ (as the supporting electrolyte), were analysed using cyclic voltammetry. Typical cyclic voltammograms (CVs) for both compounds are given in Figure 1a and 1b. For tryptophan, a two electron process, which involve two irreversible oxidation peaks at 0.770 V and 0.885 V *vs*. SCE, are observed, whereas, in the case of histidine, no electrochemical oxidation or reduction processes are noticed within the electrochemical window. These results agree with previously reported electrochemical data under similar experimental conditions. [42]

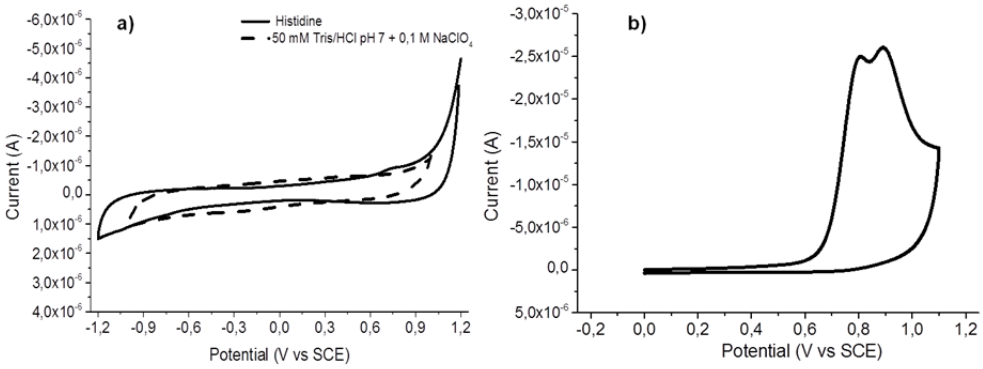

Figure 1. Cyclic voltammetry in an aqueous solution of 50 mM Tris/HCl pH 7 + 0.1 M $NaClO_4$ on a glassy carbon disk (diameter 1 mm) of a) histidine 10 mM (solid line. Scan range 0.0/1.2/–1.2/0.0 V); b) 10 mM tryptophan (scan range 0.0/1.1/0.0 V). All

measurements are referred to saturated calomel electrode (SCE). Scan Rate (V): 0.5 V s^{-1}.

Once established that tryptophan is the only electroactive amino acid, three different solutions of pure tripeptide composed of alternating histidine and tryptophan amino acids (namely **HWH**, **Ac-HWH**, **WHH** and **HHW**; see Scheme 2) were analysed using CV. For all the tripeptides, the CVs showed a two-electron irreversible oxidation wave at c.a. 0.78 *vs*. SCE (Figure 2). This oxidation wave corresponds to the oxidation of the tryptophan residue, as can be clearly deduced from the peak potential (E_{pa}) and current peak values (I_{pa}) (See Table S3).

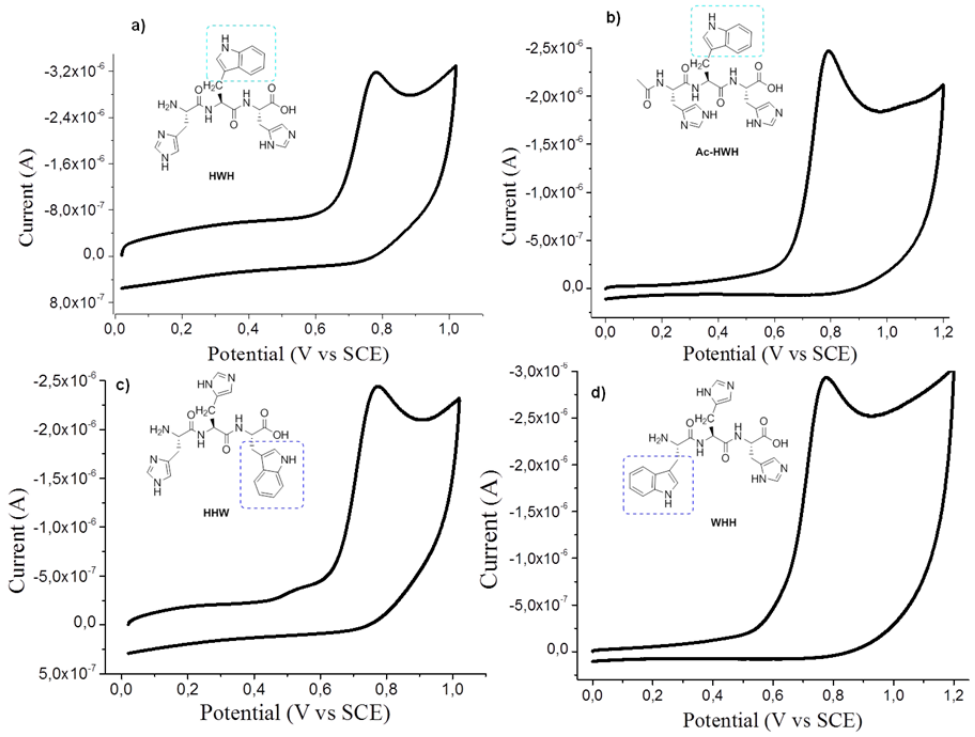

Figure 2. Cyclic voltammetry of different peptides (1 mM) in an aqueous solution of 50 mM Tris/HCl pH 7 + 0.1 M $NaClO_4$ on a glassy carbon disk (diameter 1 mm). Scan Rate: 0.5 V s^{-1} of a) **HWH** b) **Ac-HWH** c) **HHW** and d) **WHH**. All measurements are referred to a saturated calomel electrode (SCE).

Electrochemical properties of Cu(II)-tripeptides

To calibrate the working electrode and to evaluate the electrochemical set-up used for the present studies, a fresh solution of $CuCl_2 \cdot 2H_2O$ in an aqueous solution of 50 mM Tris/HCl pH 7 + 0.1 M $NaClO_4$ was first analysed. Figure 3 shows that the electrochemical reduction of Cu^{II} to Cu^{I} is reversible (E^o = –0.08 V *vs*. SCE (1)) and

relatively slow (ΔEp = 80 mV), which is in good agreement with previous data reported in the literature. [43]

$$Cu^{II} + 1\ e^- \rightleftharpoons Cu^{I} \quad E^0 = -0{,}08\ V\ (vs\ SCE) \qquad (1)$$

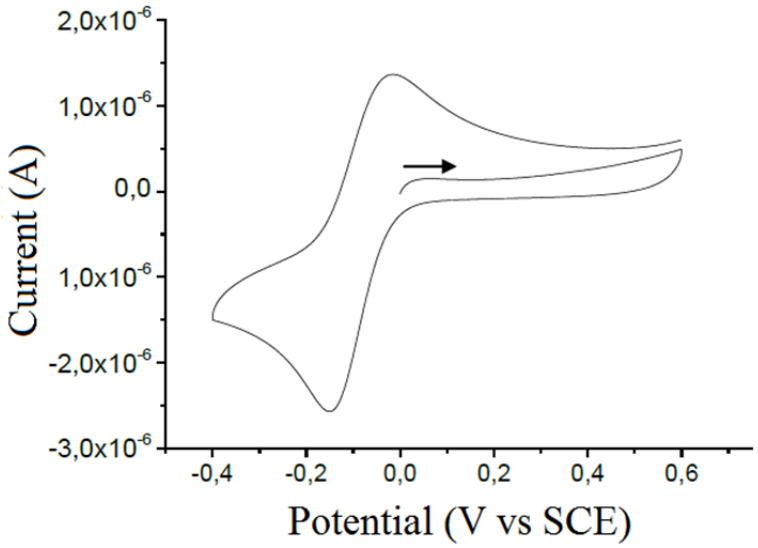

Figure 3. Cyclic voltammetry of 1 mM $CuCl_2 \cdot 2H_2O$ in an aqueous solution of 50 mM Tris/HCl pH 7 + 0.1 M NaClO4 on a glassy carbon disk (diameter 1mm). 0.3 V s^{-1} (scan range 0.0/0.6/–0.4/0.6 V). All measurements are referred to a saturated calomel electrode (SCE).

Cyclic voltammograms of the complexes **Cu^{II}–HAH**, **Cu^{II}–HWH**, **Cu^{II}–Ac-HWH**, **Cu^{II}–HHW** and **Cu^{II}-WHH** are depicted in Figure 4. It can be observed that the electrochemical behaviour of the Cu^{II}–peptide complexes exhibits significant differences, which are ascribed to the distinct peptidic sequences or, in other words, to the binding mode of the different tripeptides.

Cu^{II}–HAH and **Cu^{II}–HWH:** At low scan rates, the complex **Cu^{II}–HWH** showed a two one-electron-electron oxidation wave at respectively 0.67 V and 0.78 V *vs*. SCE, in an anodic scan (Figure 4). The first peak corresponds to the oxidation of Cu^{II} to Cu^{III}, whereas the second one is attributed to the oxidation of the tryptophan moiety, as described in previous studies performed on similar compounds.[44-47]

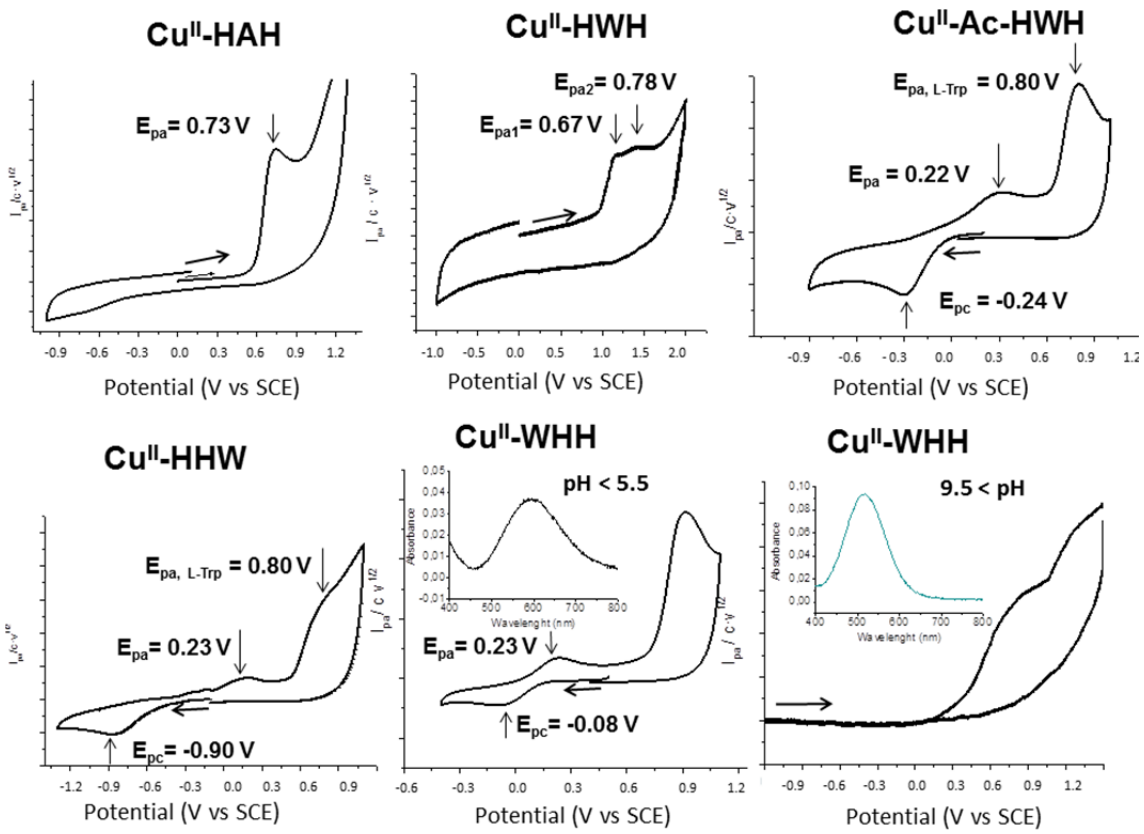

Figure 4. Cyclic voltammetry of 1 mM Cu^{II}/tripeptide in an aqueous solution of 50 mM Tris/HCl pH 7 + 0.1 M $NaClO_4$ on a glassy carbon disk (diameter 1 mm): **Cu^{II}–HAH** (v: 0.5 V s^{-1}); **Cu^{II}–HWH** (v: 0.5 V s^{-1}); **Cu^{II} –Ac-HWH** (v: 0.3 V s^{-1}); **Cu^{II}–HHW** (v: 0.3 V s^{-1}); **Cu^{II}–WHH** (v: 0.3 V s^{-1} pH = 4.8); **Cu^{II}–HHW** (v: 0.3 V s^{-1}, pH = 10.2). Inset: Absorption spectra of the **Cu^{II}–WHH** under the above-mentioned conditions. All measurements are referred to a saturated calomel electrode (SCE). The current values obtained were first normalised with respect to the concentration and the scan rate ($Ip/c.v^{1/2}$).

In the case of **Cu^{II}–HAH**, the oxidation of Cu^{II} to Cu^{III} at 0.73 V *vs*. SCE is the only electrochemical process observed since there is no electroactive amino acid present in the peptidic sequence. No cathodic processes were observed up to –1.2 V for these metallocomplexes, which means that the reduction process of Cu^{II} to Cu^{I} must happen at more negative electrochemical potentials. Moreover, high scan-rate cyclic voltammograms were performed to determine the standard potential (Eº) of the Cu^{III}–Cu^{II} electron transfer. A single one-electron reversible electron transfer was observed at 100 V s^{-1} and 5 V s^{-1} for **Cu^{II}–HWH** and **Cu^{II}–HAH**, respectively (Figure S1), allowing to calculate the Eº as the half-sum between forward and reversed peak potentials and the lifetime of the Cu^{III} complexes (Scheme 3). It should be noted that the absence of tryptophan in the peptidic sequence increases the stability of the Cu^{III}

complexes formed upon oxidation. This fact can be easily understood considering the oxidation potential of tryptophan, as an intramolecular electron transfer occurs between the Cu^{III} and the tryptophan, leading to tryptophan cation radical.

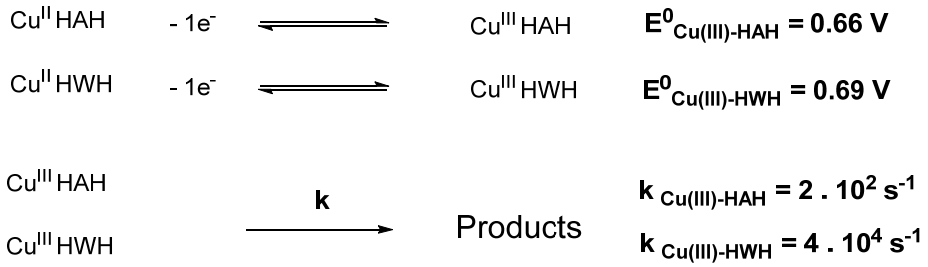

Scheme 3 Electrochemical data of **Cu^{II}–HWH** and **Cu^{II}–HAH**

To determine which coordination mode provides the electrochemical properties observed for these complexes, and to assess how much different coordination environments would influence the electrochemical behaviour, DFT (B3LYP-D3) calculations were carried out for different configurations. Possible configurations were built considering the information obtained from NMR experiments,[48] which indicated that the probable coordinating sites are the N^{term}, His1, His3, N^- from the deprotonated amide of the backbone or the O from the carbonyl group of the backbone. Since minor differences are expected among the two complexes, the exploration of different binding modes was first investigated for **Cu^{II}-HAH**. Four major configurations were considered from a computational point of view: i) configuration **1**, involving the N^{term}, His1, His3, the carboxylate group and the carbonyl O of Ala2, ii) configuration **2**, involving the N^{term}, deprotonated amide, the carbonyl O of Ala2 and His3, iii) configuration **3**, corresponding to the ATCUN motif (see Scheme 1) and involving the N^{term}, His3 and the two deprotonated N amides and finally, iv) configuration **4**, with His1, His3, the deprotonated N^- amide and the carbonyl O of Ala2 as binding sites. For all configurations, coordination through either the δ or ε nitrogen atom of the imidazole unit was considered.

The most stable **Cu^{II}–HAH** structures for each configuration are given in Figure 5, along with the computed standard reduction potential. All other **Cu^{II}–HAH** structures, and their relative stabilities are given in Figure S2 of the SI. The optimized **Cu^{II}-HAH** structures show either a pentacoordinated square-pyramidal or a tetracoordinated distorted square-planar environment, and a Cu spin density of 0.7-0.8, in agreement with the d^9 electronic configuration of Cu^{II}. Noteworthy, the calculations

indicate that the imidazole group prefers to coordinate through the δ nitrogen, since this allows the formation of five- or six-membered rings between consecutive coordination sites, and a more effective σ interaction with the metal cation. Among the different configurations considered, only configuration **3**, corresponding to the ATCUN motif, exhibits a SRP value (–1.73 V) that is compatible with the experimental observations. It can be noticed that, as mentioned above, no cathodic processes were observed up to –1.2 V, indicating that the reduction process of Cu^{II} to Cu^{I} should occur at more negative electrochemical potentials. Thus, structures **1**, **2** and **4** with SRP values of –0.07, –0.11 and -0.11 V (*vs* SCE), respectively, can be discarded.

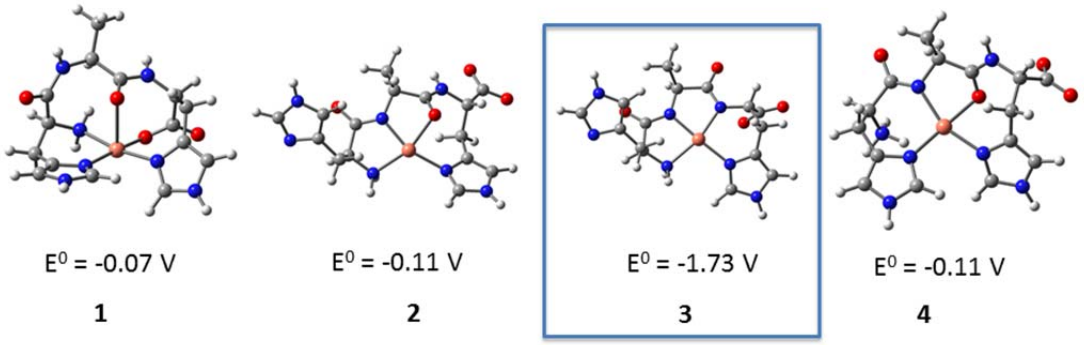

Figure 5. B3LYP-D3 optimized structures for different possible coordination environments for the complex **Cu^{II}-HAH** and computed SRP. The most plausible coordination is highlighted.

The SRP of **Cu^{II}–HWH** was computed considering the ATCUN configuration **3** and performing a conformational search of the W lateral chain orientation. Several minima with the indole moiety at different orientations, either exposed to the solvent or interacting with the metal cation, were located. The most stable structure is shown in Figure 6, whereas all other structures are given in Figure S3 of the SI. SRPs were computed to lie within the range –1.79 to –1.56 V, the structure with the indole moiety interacting with Cu^{II} showing the lowest values. On the other hand, computed values for Cu^{II}-to-Cu^{III} and tryptophan oxidations (0.60 and 0.74 V, respectively) are in very good agreement with the experimental values 0.67 and 0.78 V, respectively. It can be pointed out here that a computational accurate description of a $Cu^{II/III}$ couple is difficult since Cu^{III} complexes, with Cu in a d^8 electronic configuration in its singlet state, appear to be better described with functionals with low percentage of exact exchange, whereas Cu^{II} complexes seem to require larger percentages of exact exchange to diminish the effects of self-interaction error.[49-50]

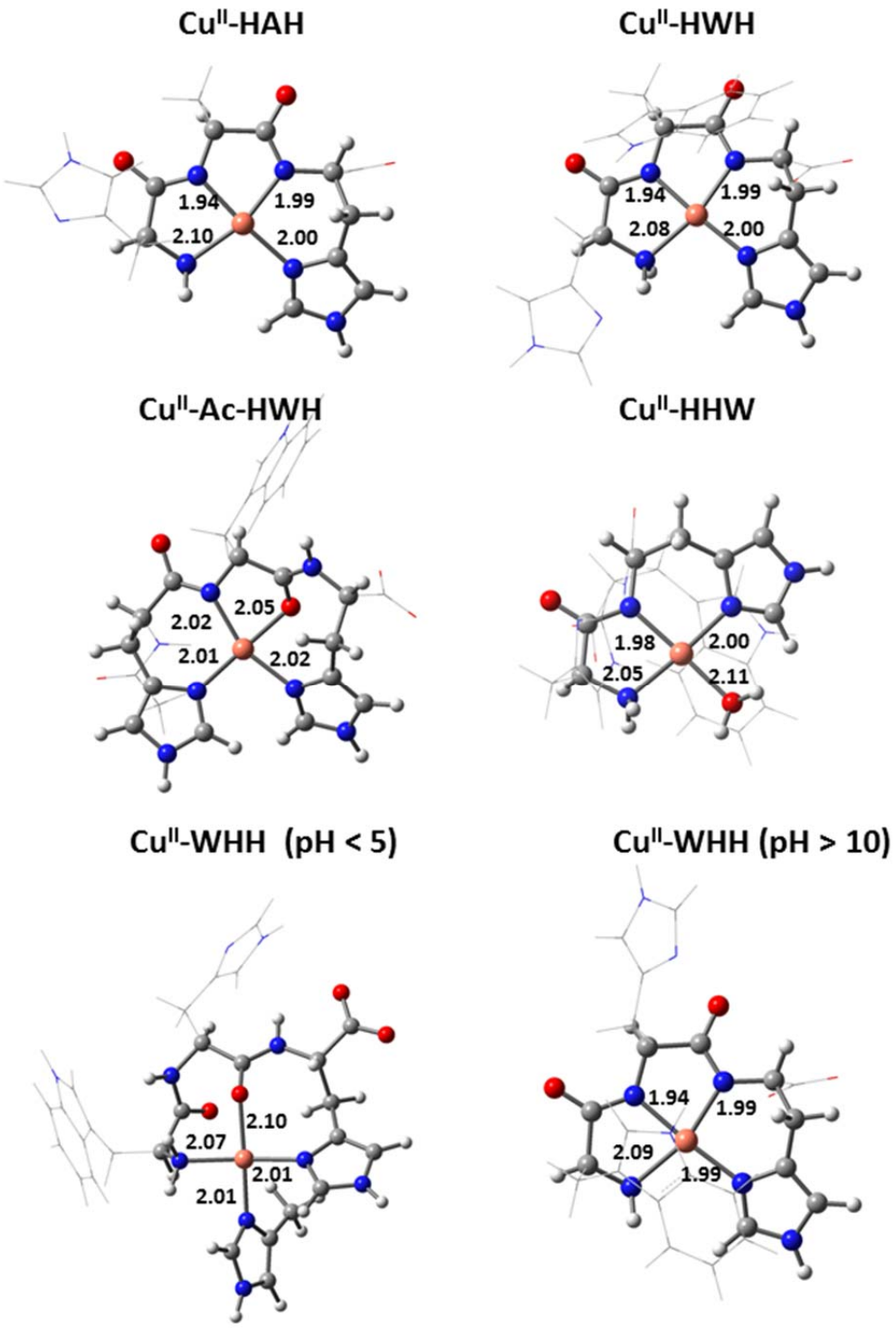

Figure 6. DFT proposed structures for Cu^{II}-tripeptides complexes. For clarity, atoms of the coordination sphere are shown as balls, whereas the remaining ones are shown as sticks. Distances are in Å.

Cu^{II}-Ac-HWH and Cu^{II}-HHW: The electrochemical behaviour observed for the complexes **Cu^{II}–Ac-HWH** and **Cu^{II}–HHW** is totally different (see Figure 4). The CV of **Cu^{II}–Ac-HWH**, starting from a cathodic scan, shows a one-electron reduction peak at –0.24 V *vs*. SCE. Furthermore, in the corresponding anodic counter scan, two oxidation peaks are observed at 0.22 V and 0.80 V *vs*. SCE. Thus, for **Cu^{II}–Ac-HWH**, the reduction of Cu^{II} to Cu^{I} occurs at –0.24 V (E_{pc}), whereas the oxidation process of Cu^{I} to Cu^{II} occurs at 0.22 V (E_{pa}). This major difference, *i.e.* of ~500 mV, between the reduction (E_{pc}=-0.24 V) and oxidation potential (E_{pa} ~ 0.22 V) agrees with an irreversible electron transfer process, and is indicative of critical changes on the coordination environment of copper and a coupled chemical reaction. The last oxidation peak at 0.80 V corresponds to the oxidation of the tryptophan amino acid present in the tripeptide (Figure 4).

Similar electrochemical results were obtained for the compound **Cu^{II}–HHW**. The peak potential values obtained for the reduction of Cu^{II} to Cu^{I} were E_{pc} = –0.90 V and E_{pa} = 0.23 V *vs*. SCE, respectively. Again, this large separation, in terms of reduction and oxidation potentials, is indicative of an irreversible electron transfer (as mentioned above for **Cu^{I}–Ac-HWH**), associated to a significant change of the copper coordination environment upon reduction and a coupled chemical reaction.

DFT calculations were performed to determine the coordination properties compatible with the electrochemical observations. For the complex **Cu^{II}–Ac-HWH**, two different structures were analysed based on the binding sites proposed by NMR experiments (see Figure 7 and Figures S4-S5) (His1, His3, N^{-} from the amide or O from the carbonyl group of the backbone): i) one simulating the ATCUN-like motif with the coordination of His1 instead of the N-terminal and ii) another one involving only one deprotonated amide, the coordination of a carbonyl group and two histidines; *i.e*, a structure with a 3N1O coordination environment. Moreover, based on the previous results achieved for **Cu^{II}–HAH**, only the δ nitrogen coordination of the imidazole ring was considered (see above).

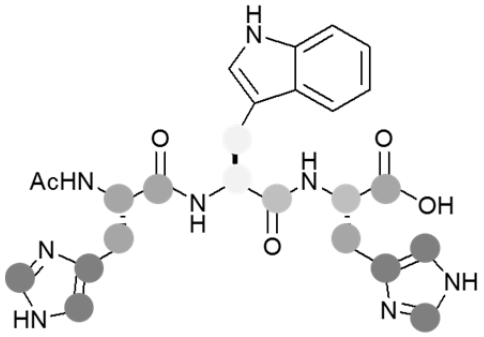

Figure 7. Schematic representation of the magnitude of NMR peak broadening upon addition of 0.01 equiv of copper(II) to **Ac-HWH** in D_2O at pH 7.4. Dark dots symbolize strongly affected signals while light dots indicate less affected signals.

The computed reduction potential for the ATCUN-like complex (Figure S6) is –1.35 V, whereas that for the 3N1O complex (Figure 6), with only one deprotonated amide, is –0.23 V. The data for the latter complex is in very good agreement with the value of –0.24 V observed by CV for the one-electron reduction peak E_{pc}. Thus, these results suggest that, in order to achieve the ATCUN like coordination with two deprotonated amides, the binding of two consecutive five-membered rings are necessary to provide the required stabilization, so as the coordination of the amino terminal group. Furthermore, the calculations show that for this complex, the Cu^{II}-to-Cu^{I} reduction induces an important elongation of the Cu–O bond distance, from 2.05 Å to 3.52 Å (Figure 6 and Figure S7 of SI). That is, the initial distorted square-planar (3N1O) coordination geometry of the **Cu^{II}–Ac-HWH** complex changes to a trigonal planar molecular geometry (Figure 8), where the copper interacts with 3 nitrogen atoms (3N). This is similar to that found for 3N1O Cu^{II}-Aβ(1-16), for which molecular dynamics simulations indicated that CO decoordination occurs rapidly at t = 0.2 ps.[51]

Calculations show that oxidation of the tricoordinated **Cu^{I}–AcHWH** complex is not reversible, resulting in a tricoordinated **Cu^{II}** species that is slightly less stable than the tetracoordinated one (Figure 6). Such changes on the coordination environment, however, do not explain the significant difference (of ~500 mV) observed between E_{pc} and E_{pa}, since the computed oxidation and reduction potential differ by less than 50 mV, which suggest that a coupled chemical reaction, such as amide protonation, should also be involved in the reduction process (Figure 8). Indeed, the oxidation potential of **Cu^{I}-WHH** complex at low pH, and thus, with no amides deprotonated provides also a E_{pa} value of 0.23 V (see below).

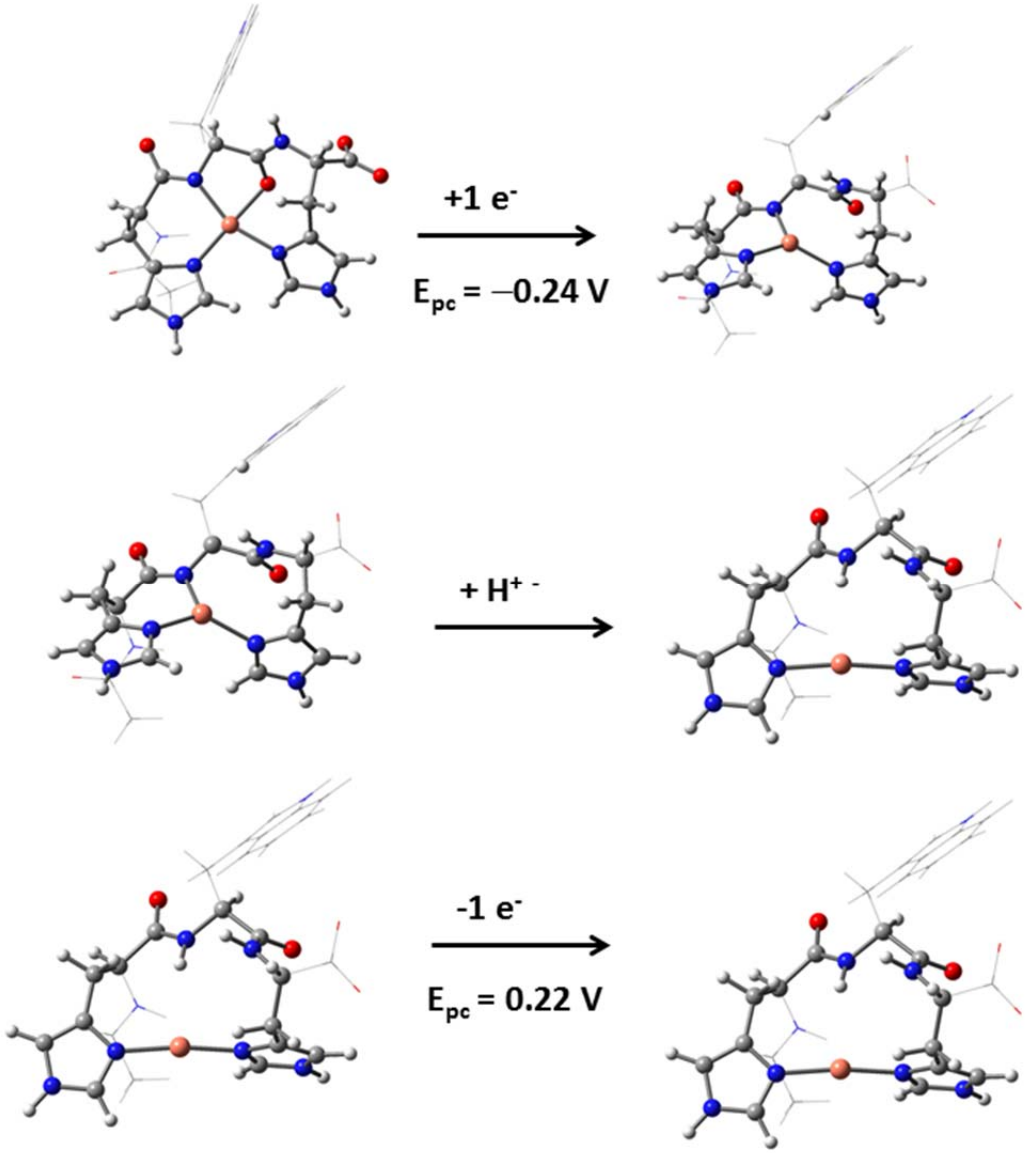

Figure 8. Proposed structures for the irreversible Cu^{II}/Cu^{I} process of **Cu^{II}-AcHWH**

For the complex **Cu^{II}–HHW**, the single-crystal X-Ray could be determined (see SI for the crystallographic data; Table S2). As evidenced in Figure 9, this complex does not present ATCUN coordination. The copper ion is coordinated by two peptides. Thus, the metal centre is in a square-pyramidal environment, the basal plane consisting of four nitrogen atoms and the apical position being occupied by a water molecule. One of the tripeptides acts as tridentate ligand through an N-terminal amino group (N6), a deprotonated N amide function (N5) and a histidine nitrogen atom (N3; histidine at position 2). A second tripeptide completes the basal plane of the square pyramid *via* the binding of a second histidine nitrogen atom (N7f; histidine at position 1).

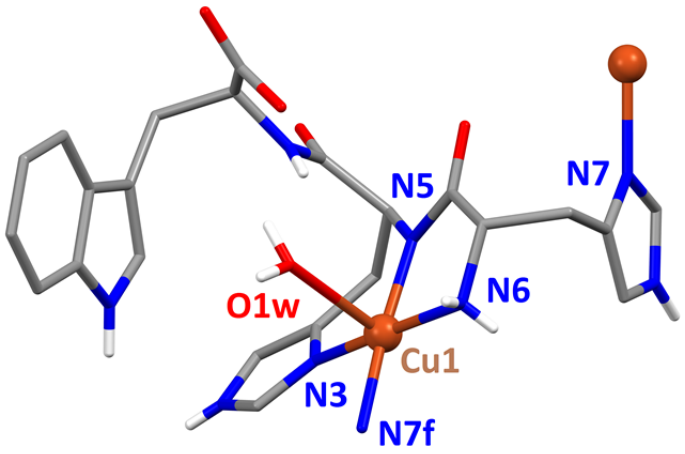

Figure 9. Representation of the molecular structure of complex **Cu^{II}–HHW** with partial atom-numbering scheme. Only the hydrogen atoms of the water molecule, coordinated amino group and amide, imidazole and indole nitrogens are shown for clarity. Symmetry operation: f = 1/2–x, 1–y, –1/2+z.

The water molecule is coordinated at a long distance, namely Cu1−O1w = 2.619(4) Å (see Table S2). The coordination angles reflect an almost perfect square-pyramidal geometry, with a τ factor of 0.02.[52] In the solid state, a 1D chain is observed that results from the binding of His1 to an adjacent copper unit (Figure S8). In solution, the solvent may displace His1, disrupting the coordination chain. To embrace all possibilities, we have theoretically considered two cases, namely (i) Cu^{II} bound to one **HHW** peptide with a water molecule at the fourth position (3N1O environment), and (ii) Cu^{II} bound to two **HHW** peptides, as in the X-ray crystal structure, with one histidyl imidazole at the fourth position (4N environment). Again, only δ nitrogen coordination of the histidines was considered.

The computed reduction potential for the 3N1O and 4N structures are –0.80 V and –1.04 V, respectively, in good agreement with the peak potential value of –0.90 V obtained experimentally. Although both the 3N1O and 4N complexes exhibit relatively similar values, the 3N1O coordination set (Figure 6), with one water solvent molecule bound to the metal centre, is expected to be the major species present in solution, under the experimental conditions applied. The reduction of **Cu^{II}-HHW** induces the decoordination of the O-donor ligand, as reflected by the Cu–O distance increase from 2.11 Å to 3.00 Å (Figure 6 and Figure S7 of SI), which leads to a T-shaped tricoordinated structure. As for **Cu^{II}–Ac-HWH,** the significant difference observed

between E_{pa} and E_{pc} in the electrochemical experiments suggest that, besides the changes in copper coordination, reduction is accompanied by a protonation of N^-.

Cu^{II}–WHH: Previous results were sufficiently encouraging to not only extend the study to other copper complexes, but also to obtain important quantitative data related to the copper(II)-bound motif. Thus, the **Cu^{II}-WHH** complex, whose coordination environment is pH dependent, was selected to evaluate the reliability, consistency, and accuracy of CV to determine the geometry and coordination environment of Cu(II) metallopeptide complexes in solution.

Figure 4 shows the absorption and cyclic voltammograms measured for the different copper coordination modes at different pH values. At pH below 5.5, the optical and redox properties characterise a copper complex with a 3N donor set ($\lambda_{abs,max}$= 600 nm and **Cu^{II}–WHH** to **Cu^{I}–WHH** reduction). It is worth noting that the cathodic and anodic peak potential values are significantly separated (by ~300 mV; E_{pc} = –0.08 V and E_{pa} = 0.23), although not as much as for **Cu^{II}–Ac-HWH** and **Cu^{II}-HHW**, which suggests that an important conformational rearrangement coupled to the electron transfer takes place. Note that in contrast to **Cu^{II}–Ac-HWH** and **Cu^{II}-HHW**, no reprotonation can be involved at this low pH. The oxidation of the tryptophan residue is also detected in the corresponding anodic counter scan.

Several structures were examined using DFT simulations to determine which one provides the electrochemical behaviour observed experimentally. In particular, structures analogous to those tested for **Cu–HHW**, with one deprotonated amide, were considered. Furthermore, since the cathodic potential for **Cu–WHH** at low pH is significantly higher than that of **Cu–HHW** complexes, structures with no deprotonated amides were also tested. These structures involve the coordination of the N^{term}, a carbonyl oxygen, His3, and a water molecule or a methyl imidazole, simulating the coordination of a histidine from another peptide, at the fourth position. Among all structures considered (see Figure S9 of SI), those with no deprotonated amides, either with a 2N2O-donor set including a water molecule at the fourth position or a 3N1O-donor set involving an imidazole at the fourth position (Figure 6 and Figure S9), provide a reduction potential value (0.26 V for 2N2O and 0.11 V for 3N1O), the latter being in better agreement with the experimental value (–0.08 V).

Upon base-induced modification of the coordination environment of **Cu^{II}–WHH**, clear changes of the optical and redox properties were observed. As expected, at pH around 9.5, the visible absorption band is shifted from 600 nm to 525 nm. Furthermore, as observed for **Cu^{II}–HAH** and **Cu^{II}–HWH**, two one-electron oxidation peaks at 0.65 V and 0.79 V *vs*. SCE are detected. As previously mentioned, those two peaks are associated with respectively, the oxidation of the ATCUN-type complex **Cu^{II}–WHH** to its **Cu^{III}** form and to the oxidation of tryptophan. Furthermore, due to the high stability of the ATCUN coordination mode, no cathodic processes are observed up to –1.2 V. As a matter of fact, and like for previous metallocomplexes (see above), DFT calculations for the ATCUN **Cu^{II}–WHH** compound (Figure 6) give a reduction potential of –1.77 V, below the electrochemical window.

Concluding remarks

The results achieved in the present study show that the electrochemical behaviour of copper-peptide complexes is highly dependent on the peptidic sequence. The differences observed are directly related to the metal coordination environment, as clearly demonstrated by comparing experimental electrochemical results with those computed using DFT electronic structure methods for different structures. The electrochemical properties associated with the different coordination environments are summarized in Table 1.

The main redox fingerprint for a copper(II)-ATCUN complex is (i) the presence of an oxidation peak at c.a. 0.7 V *vs*. SCE, ascribed to the oxidation of Cu(II) to Cu(III), and (ii) the absence of cathodic processes up to –1.2 V (very high stability towards copper reduction). This behaviour is associated to the formation of a very stable square planar (5,5,6)-membered chelate rings (ATCUN motif), in which the terminal amino group, the two deprotonated amides and the Nδ of His3 coordinate the metal cation. The rigidity of the coordination environment and the presence of two negatively charged coordination sites hinder the reduction process, thereby being inactive within the electrochemical window.

Table 1. Electrochemical data for Cu^{II}-tripeptides complexes in different solutions of 50 mM Tris/HCl pH 7.4 containing 0.1 M $NaClO_4$ at 20 °C.

	Cu(II)-tripeptides Complexes – ATCUN Coordination Mode				
Compound	**Coordination mode**	**$E_{pc,\ Cu(II)-Cu(I)}$ (V)[a]**	**$E_{pa,\ Cu(II)-Cu(III)}$ (V)[a]**	**Number of deprotonated Amides**	**$E_{,\ Cu(II)-Cu(I)}$ Computed Reduction Potential**
Cu^{II}-HAH	NH_2, N^-_{am1}, N^-_{am2}, $N\delta_{H3}$	< −1.2	0.73	2	−1.73
Cu^{II}-HWH	NH_2, N^-_{am1}, N^-_{am2}, $N\delta_{H3}$	< −1.2	0.67	2	−1.79
Cu^{II}-WHH, pH=10.2	NH_2, N^-_{am1}, N^-_{am2}, $N\delta_{H3}$	< −1.2	0.67	2	−1.77
	Cu(II)-tripeptides Complexes – No ATCUN Coordination Mode				
Compound	**Coordination mode**	**$E_{pc,\ Cu(II)-Cu(I)}$ (V)[a]**	**$E_{pa,\ Cu(I)-Cu(II)}$ (V)[a]**	**Number of deprotonated Amides**	**$E_{,\ Cu(II)-Cu(I)}$ Computed Reduction Potential**
Cu^{II}-Ac-HWH	$N\delta_{H1}$,$N^-_{am1}CO_{A2}$, $N\delta_{H3}$	−0.24	0.22	1	−0.23
Cu^{II}-HHW	NH_2, N^-_{am1}, $N\delta_{H3}$, H_2O NH_2, N^-_{am1} $N\delta_{H3}$ Imi	−0.90	0.23	1	−0.80 −1.04
Cu^{II}-WHH, pH=4.2	NH_2, CO_{A2}, $N\delta_{H3}$ H_2O NH_2, CO_{A2}, $N\delta_{H3}$ Imi	−0.08	0.23	0	0.26 0.11

[a] Given peak potential values (Ep) *vs*. SCE and measured at v = 0.1 $V.s^{-1}$; The number of electrons involved in the first oxidation process was determined by comparison with solutions of $CuCl_2$ (a very well-known one-electron oxidation compound in terms of cyclic voltammetry).

In contrast, for non-ATCUN copper(II)-peptide complexes, the main electrochemical feature is a reductive irreversible electron-transfer process from Cu(II) to Cu(I), accompanied with structural changes of the metal coordination sphere and reprotonation of the amide. In these cases, DFT simulations indicate that the Cu^{II} complex would enclose only one or none deprotonated amide and a less rigid coordination environment, which results in a much higher reduction potential. Furthermore, according to DFT calculations, the structural changes induced upon reduction mainly correspond to the decoordination of one of the ligands, producing a

tricoordinated complex, and to the amide reprotonation, which would be responsible for the observed difference of at least 500 mV between E_{pc} and E_{pa}.

Overall, the results obtained in this study show that redox potentials are deeply affected by the presence of negatively charged ligands in the coordination sphere. In this regard, ATCUN complexes, with two deprotonated amides and a rigid coordination sphere, are the ones that exhibit the lowest SRP values (around –1.7 V). It is worth noting that the amide deprotonation is costly (pKa ~ 15);[53] thus, such proton abstraction will only occur if the required energetic cost is compensated by a high stability of the resulting complex, which is the case for the ATCUN motif. If the peptide coordination cannot generate an ATCUN motif, either because there is not an N-terminal group (like for **Cu^{II}–Ac-HWH**) or there is no histidine at the third peptidic position (*e.g.* **Cu^{II}–HHW**), the resulting complex with only have one deprotonated amide that is characterized by a much higher E_{pc} (from -0.9 to –0.2 V Table 1). Noteworthy, for the compound **Cu^{II}–WHH**, for which both the N-terminal ligand and the histidine at position 3 are available, the ATCUN motif is only formed at high pH. Indeed, for this complex two major species have been detected: one at low pH (< 5), with no deprotonated amides, and (E_{pc} ~ 0 and E_{pa} ~ 0.2 V)) and another one at high pH (> 10) with an ATCUN motif, both species coexisting at intermediante pH. This suggests that the peptidic sequence, *e.g.* the nature of the aminoacids involved (for instance, the tryptophan at position 1 or/and the histidine at position 2 for this complex), also plays a key role regarding the (electrochemical) properties of the corresponding complex.

Finally, it is worth noting that previous electrochemical studies for Cu^{II} complexes with larger peptides have shown a similar behaviour.[44, 54-55] For instance, for Cu^{II}-Aβ(4-16), with a His residue in the third position, the CV indicates that the complex does not yield any electrochemical Cu^{II}/Cu^{I} redox activity due to the formation of an ATCUN binding mode.[44] In contrast, for Cu^{II}-Aβ(1-16), with three His and a carbonyl group,[53] or for Cu^{II} interacting with the octarepeat segment of the prion protein with four His[55] in the coordination sphere, the CV is very similar to that obtained for Cu^{II}-WHH at low pH.

It is important to highlight that the use of CV, using glassy carbon as a working electrode, has been introduced in the present work as an ideal and rapid tool for the determination of the redox properties of Cu(II) metallopeptides. It should be

emphasised that, by using CV (since it is a non-destructive electrochemical technique), it is possible to have access to all the above-mentioned information by using only one single aliquot of 5 mL (or less) of solution. Besides, the use of cyclic voltammetry allows to obtain valuable thermodynamic data (E^o), which are very useful for a better understanding of the redox properties of complexes that may be involved in relevant catalytic processes.

Acknowledgements

The authors gratefully acknowledge financial support from MINECO (projects CTQ2014-59544-P, CTQ2014-55293-P, CTQ2015-70371-REDT and CTQ2015-65439-P) and the Generalitat de Catalunya (projects and 2014SGR-482). MS acknowledges the Generalitat de Catalunya for the 2011 ICREA Academia award. ABC acknowledges European Union's Horizon 2020 research and innovation programme for her Marie Skolodowska-Curie grant No. 656820. This research used resources of the Advanced Light Source, which is a DOE Office of Science User Facility under contract no. DE-AC02-05CH11231. The authors also gratefully acknowledge Iluminada Gallardo for very fruitful discussions.

References

[1] J. W. Dixon, B. Sarkar, *J. Biol. Chem.* **1974**, *249*, 5872-5877.
[2] C. Harford, B. Sarkar, *Acc. Chem. Res.* **1997**, *30*, 123-130.
[3] R. Sankararamakrishnan, S. Verma, S. Kumar, *Prot-Struct Funct Bioinf* **2005**, *58*, 211-221.
[4] G. Gasmi, A. Singer, J. FormanKay, B. Sarkar, *J. Pept. Res.* **1997**, *49*, 500-509.
[5] S. Melino, M. Gallo, E. Trotta, F. Mondello, M. Paci, R. Petruzzelli, *Biochemistry* **2006**, *45*, 15373-15383.
[6] D. J. McKay, B. S. Renaux, G. H. Dixon, *Eur. J. Biochem.* **1986**, *156*, 5-8.
[7] T. Peters, *Biochim. Biophys. Acta* **1960**, *39*, 546-547.
[8] D. W. Appleton, B. Sarkar, *J. Biol. Chem.* **1971**, *246*, 5040-5046.
[9] T. Peters, Blumenst.Fa, *J. Biol. Chem.* **1967**, *242*, 1574-1578.
[10] K. P. Neupane, A. R. Aldous, J. A. Kritzer, *J. Inorg. Biochem.* **2014**, *139*, 65-76.
[11] J. P. Laussac, B. Sarkar, *Biochemistry* **1984**, *23*, 2832-2838.
[12] W. Bal, M. Sokolowska, E. Kurowska, P. Faller, *Biochimica Et Biophysica Acta-General Subjects* **2013**, *1830*, 5444-5455.
[13] Y. Jin, J. A. Cowan, *J. Am. Chem. Soc.* **2005**, *127*, 8408-8415.
[14] C. R. Munteanu, J. M. Vázquez, J. Dorado, A. P. Sierra, A. Sánchez-González, F. J. Prado-Prado, H. González-Díaz, *J. Proteom. Res.* **2009**, *8*, 5219-5228.
[15] S. H. Chiou, *J. Biochem.* **1983**, *94*, 1259-1267.

[16] E. Kimoto, H. Tanaka, J. Gyotoku, F. Morishige, L. Pauling, *Cancer Research* **1983**, *43*, 824-828.
[17] D. P. Mack, P. B. Dervan, *Biochemistry* **1992**, *31*, 9399-9405.
[18] J. Torreilles, M. C. Guerin, A. Slaouihasnaoui, *Free Rad. Res. Comm.* **1990**, *11*, 159-166.
[19] B. Cuenoud, T. M. Tarasow, A. Schepartz, *Tetrahedron Lett.* **1992**, *33*, 895-898.
[20] N. H. Gokhale, J. A. Cowan, *Chem. Comm.* **2005**, 5916-5918.
[21] K. C. Brown, S. H. Yang, T. Kodadek, *Biochemistry* **1995**, *34*, 4733-4739.
[22] E. Basle, N. Joubert, M. Pucheault, *Chemistry & Biology* **2010**, *17*, 213-227.
[23] S. Meunier, E. Strable, M. G. Finn, *Chemistry & Biology* **2004**, *11*, 319-326.
[24] J. C. Joyner, J. A. Cowan, *Braz. J. Med. Biol. Res.* **2013**, *46*, 465-485.
[25] K. D. Mjos, C. Orvig, *Chem. Rev.* **2014**, *114*, 4540-4563.
[26] S. Bradford, J. A. Cowan, *Chem. Comm.* **2012**, *48*, 3118-3120.
[27] S. S. Bradford, M. J. Ross, I. Fidai, J. A. Cowan, *ChemMedChem* **2014**, *9*, 1275-1285.
[28] Y. P. Ginotra, S. N. Ramteke, R. Srikanth, P. P. Kulkarni, *Inorg. Chem.* **2012**, *51*, 7960-7962.
[29] B. Alies, C. Hureau, P. Faller, *Metallomics* **2013**, *5*, 183-192.
[30] D. Andrae, U. HauBermann, M. Dolg, H. Stoll, H. PreuB, *Theor. Chim. Acta.* **1990**, *77*, 123-141.
[31] A. D. Becke, *J. Chem. Phys.* **1993**, *98*, 5648-5652.
[32] C. Lee, W. Yang, R. G. Parr, *Phys. Rev. B* **1988**, *37*, 785-789.
[33] S. Grimme, J. Antony, S. Ehrlich, H. Krieg, *J. Chem. Phys.* **2010**, *132*, 154104-154104.
[34] P. J. Hay, W. R. Wadt, *J. Chem. Phys.* **1985**, *82*, 299-310.
[35] L. E. Roy, P. J. Hay, R. L. Martin, *J. Chem. Theor. Comp.* **2008**, *4*, 1029-1031.
[36] A. W. Ehlers, M. Böhme, S. Dapprich, A. Gobbi, A. Höllwarth, V. Jonas, K. F. Köhler, R. Stegmann, A. Veldkamp, G. Frenking, *Chem. Phys. Lett.* **1993**, *208*, 111-114.
[37] A. V. Marenich, C. J. Cramer, D. G. Truhlar, *J. Phys. Chem. B* **2009**, *113*, 6378-6396.
[38] M. J. Frisch, G. W. Trucks, H. B. Schlegel, G. E. Scuseria, M. A. Robb, J. R. Cheeseman, G. Scalmani, V. Barone, B. Mennucci, G. A. Petersson, H. Nakatsuji, M. Caricato, X. Li, H. P. Hratchian, A. F. Izmaylov, J. Bloino, G. Zheng, J. L. Sonnenberg, M. Hada, M. Ehara, K. Toyota, R. Fukuda, J. Hasegawa, M. Ishida, T. Nakajima, Y. Honda, O. Kitao, H. Nakai, T. Vreven, J. A. Montgomery Jr, J. E. Peralta, F. Ogliaro, M. Bearpark, J. J. Heyd, E. Brothers, K. N. Kudin, V. N. Staroverov, R. Kobayashi, J. Normand, K. Raghavachari, A. Rendell, J. C. Burant, S. S. Iyengar, J. Tomasi, M. Cossi, N. Rega, J. M. Millam, M. Klene, J. E. Knox, J. B. Cross, V. Bakken, C. Adamo, J. Jaramillo, R. Gomperts, R. E. Stratmann, O. Yazyev, A. J. Austin, R. Cammi, C. Pomelli, J. W. Ochterski, R. L. Martin, K. Morokuma, V. G. Zakrzewski, G. A. Voth, P. Salvador, J. J. Dannenberg, S. Dapprich, A. D. Daniels, Ö. Farkas, J. B. Foresman, J. V. Ortiz, J. Cioslowski, D. J. Fox, pp. Gaussian, Inc., Wallingford CT, 2009-Gaussian, Inc., Wallingford CT, 2009.
[39] N. Hewitt, A. Rauk, *J. Phys. Chem. B* **2009**, *113*, 1202-1209.
[40] SADABSandSAINT, Madison, Wisconsin USA, Bruker AXS Inc.
[41] G. M. Sheldrick, *Acta Crystallogr C* **2015**, *71*, 3-8.
[42] X. H. Xia, Z. X. Zheng, Y. Zhang, X. J. Zhao, C. M. Wang, *Sensor Actuat B-Chem* **2014**, *192*, 42-50.
[43] L. Sanz, J. Palma, E. Garcia-Quismondo, M. Anderson, *J Power Sources* **2013**, *224*, 278-284.
[44] M. Mital, N. E. Wezynfeld, T. Fraczyk, M. Z. Wiloch, U. E. Wawrzyniak, A. Bonna, C. Tumpach, K. J. Barnham, C. L. Haigh, W. Bal, S. C. Drew, *Angew Chem Int Edit* **2015**, *54*, 10460-10464.
[45] C. Hureau, H. Eury, R. Guillot, C. Bijani, S. Sayen, P. L. Solari, E. Guillon, P. Faller, P. Dorlet, *Chem. Eur. J.* **2011**, *17*, 10151-10160.
[46] L. Guilloreau, S. Combalbert, A. Sournia-Saquet, H. Mazarguil, P. Faller, *ChemBioChem* **2007**, *8*, 1317-1325.

[47] C. Hureau, C. Mathe, P. Faller, T. A. Mattioli, P. Dorlet, *J Biol Inorg Chem* **2008**, *13*, 1055-1064.
[48] A. B. Caballero, L. Terol-Ordaz, A. Espargaró, G. Vázquez, E. Nicolás, R. Sabaté, P. Gamez, *Chem.- Eur. J.* **2016**, *22*, 7268-7280.
[49] R. Rios-Font, M. Sodupe, L. Rodriguez-Santiago, P. R. Taylor, *J Phys Chem A* **2010**, *114*, 10857-10863.
[50] M. Sodupe, J. Bertran, L. Rodriguez-Santiago, E. J. Baerends, *J Phys Chem A* **1999**, *103*, 166-170.
[51] A. Mirats, J. Ali-Torres, L. Rodriguez-Santiago, M. Sodupe, *Theor Chem Acc* **2016**, *135*.
[52] A. W. Addison, T. N. Rao, J. Reedijk, J. Vanrijn, G. C. Verschoor, *J Chem Soc Dalton* **1984**, 1349-1356.
[53] B. Martin, in *Met. Ions Biol. Syst., Vol. 38* (Ed.: A. S. a. H. Sigel), Marcel Dekker Inc., New York, **2001**.
[54] V. Balland, C. Hureau, J. M. Saveant, *P Natl Acad Sci USA* **2010**, *107*, 17113-17118.
[55] L. Liu, D. L. Jiang, A. McDonald, Y. Q. Hao, G. L. Millhauser, F. M. Zhou, *J. Am. Chem. Soc.* **2011**, *133*, 12229-12237.

Table of Contents Graphics